International Journal of Nanoelectronics and Materials
Volume 15 (Special Issue) December 2022 [285-292]

The Influence of Crystal Orientation Variation towards the Modal Phase Matching Condition in Lithium Niobate on Insulator Waveguide

Nor Roshidah Yusof[1,3], Norshamsuri Ali [1,3], and Piotr Kolenderski[2]

[1]Advanced Communication Engineering Centre of Excellent, UniMAP, 02000 Arau, Perlis, Malaysia
[2]Faculty of Physics, Astronomy and Informatics, Nicoulas Copernicus University in Torun, Grudziadzka 5, 87-100 Torun, Poland
[3]Faculty of Electronic Engineering Technology, Universiti Malaysia Perlis, 02000 Perlis, Malaysia

ABSTRACT

We systematically demonstrate the influence of crystal orientation towards the phase matching condition in Lithium Niobate on insulator waveguide structure. The phase matching condition is one of the important elements that required prior to the development of ultracompact photonic integrated circuit. This is achieved as the effective refractive indices of fundamental mode, TE_{00} at pump wavelength overlapped with the second order mode, TE_{20} of second harmonic wavelength. With a proper selection of crystal orientation, the perfect phase matching condition is achievable over a broader telecommunication wavelength, hence, improve the efficiency of the device. In this work, we examine the phase matching interaction over the x-, y- and z- cut LNOI crystal structure. From the numerical analysis, the significant variation of phase matching width over crystal orientation is demonstrated with x-cut LNOI shows a strong ability to achieve the modal phase matching at narrower width, allowing the realization of ultracompact waveguide fabrication. Interestingly, z-cut LNOI, offers a broader range of phase matching wavelength tunability which beneficial for the development of optical modulator. Eventually, the y-cut LNOI suit for the fabrication of the wavelength-independent optical devices such as surface acoustic waveguide.

Keywords: LNOI, modal birefringence, nonlinear material, optical waveguide

1. INTRODUCTION

Lithium niobate is known as an outstanding photonic material platform due to its excellence linear and nonlinear properties over a broad transparency window ranging from 350 nm to 5200 nm (Wong, 2002). However, the realization of high dense Photonic integrated circuit (PIC) is remained challenging in conventional Lithium Niobate (LN) wafer due to small index contrast until the recent development of Lithium Niobate on Insulator (LNOI) wafer. This emerging platform offers an exceptional opportunity for the compact and complex integration of optical component on single chip in various application such as telecommunication (Rao, 2017), optical sensing (Qi, 2020), ultrafast computing (Pang, 2018) and quantum communication (Alibart, 2016). Since then, it attracts the significant interest on the development of optical waveguide for various functionalities including racetrack resonator (Witmer, 2017), Mach-Zender modulator (Mahmoud, 2017), optical filter (Li, 2020) and entangled photon pair source and detector (Sun, 2020). The LNOI optical waveguide possess a strong modal confinement leading to higher optical intensities, which beneficial for the nonlinear optical applications. On top of that, the existence of silica layer underneath the thin film LN enable to improve the electro-optic efficiency of the waveguide, by enhancing the electrical field overlapping with the optical waveguide mode.

Owing the hard and chemically inert characteristic, LNOI, however, suffer high propagation losses resulted from poor dry etching fabrication process. Several practical etching methods have been demonstrated to overcome this constrain including ion beam enhanced etching (Lacour, 2015), deep oxide etching (Levy, 1998) and Inductively Coupled Plasma reactive ion etching (Saravi, 2021). The biggest challenge lies in fabrication of optimum waveguides which would be suited to the wavelength of interest. The crystal orientation of the anisotropic material such LN is believed to affect the feasibility of the waveguide. Unfortunately, these important features have been abandoned in recent research activities. Precise control of the nanofabrication process not only contributes to tight mode confinement but will enhance the nonlinear effect. With capability to generate the entangled photon pairs through the spontaneous parametric down-conversion in LN technology gives an incredible influence towards the realization of on-chip monolithic integrated devices (Xue, 2021). Though, the phase matching condition must be satisfied to safeguard its compatibility within a desired wavelength and nonlinear coefficient (Ye, 2020).

In this paper, we systematically investigate the phase matching condition of LNOI rib waveguide structure over the various crystal orientations. As depicted in Figure 1, the LN crystal structure is dominated by the Lithium, Li and Niobium, Nb ion. Three main cut, *x-*, *y-* and *z-* represented by the crystal direction of $[2\bar{1}\bar{1}0]$, $[1\bar{1}00]$ and [0001], respectively. On top of that, the phase matching tunability towards the waveguide's width variation is also investigated as it provides a feasible framework prior fabrication which has been poorly addressed previously.

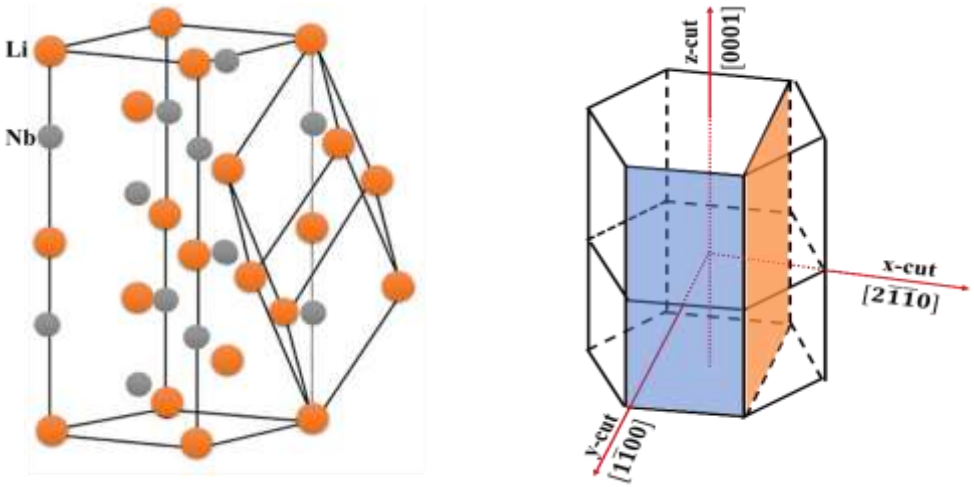

Figure 1. Left-The triclinic Lithium Niobate crystal structure which dominated by the Lithium and Niobium ion. The x-, y- and z- cut LN represented by the crystal direction of $[2\bar{1}\bar{1}0]$, $[1\bar{1}00]$ and [0001], respectively (Sanna,2010).

2. DESIGN AND SIMULATION

The electromagnetic propagation of anisotropic optical waveguide such Lithium Niobate shows a strong dependent on the material properties as well as the geometrical structure, which later contributed to the modal dispersion. Hence, a proper selection of crystal orientation and precise control of geometrical dimension enable the fabrication of low loss ultracompact waveguide structure. In this work, we systematically analyze the phase matching condition on the 500 nm thick LNOI with fixed angle, θ and etched depth, h of 75° and 400 nm, respectively. The design and simulation of the LNOI structure illustrated in Figure 2 are performed by using COMSOL Multiphysics based on the finite element method. The crystal orientation of the *x-*, *y-* and *z-*cut is distinguished by setting the transverse plane along the *xz*, *xy* and *yz* plane while electromagnetic field propagation in *y-*, *z-* and *x-* axis, accordingly. In all orientation, the *x-* and *y-* axes possess the ordinary (fast) axis whereas *z-* axis denoted as the extraordinary (slow) axis. In this case, the

extraordinary refractive indices, n_{eo} is slightly smaller compared to ordinary indices, n_o. Since LN is known as the wavelength-dependence material, the ordinary and extraordinary refractive indices of the congruent LN are modelled by using the Sellmeier dispersion relation (Zelmon, 1997). By using the finite element analysis, the Maxwell equation along with a set of boundary condition is utilized to determine the eigenmode of the waveguide. Continuously, the effective indices, n_{eff} of the confined mode is formulated in Equation 1 where β_o and κ_o denoted the mode propagation constant and free space wavenumber. The perfect propagation mode in waveguide is achieved as $n_{sio_2} < n_{eff} < n_{LN}$ and the phase matching condition is achieved when the effective refractive indices, n_{eff} at both fundamental (pump) wavelength and second harmonic (SH) wavelength are equivalent.

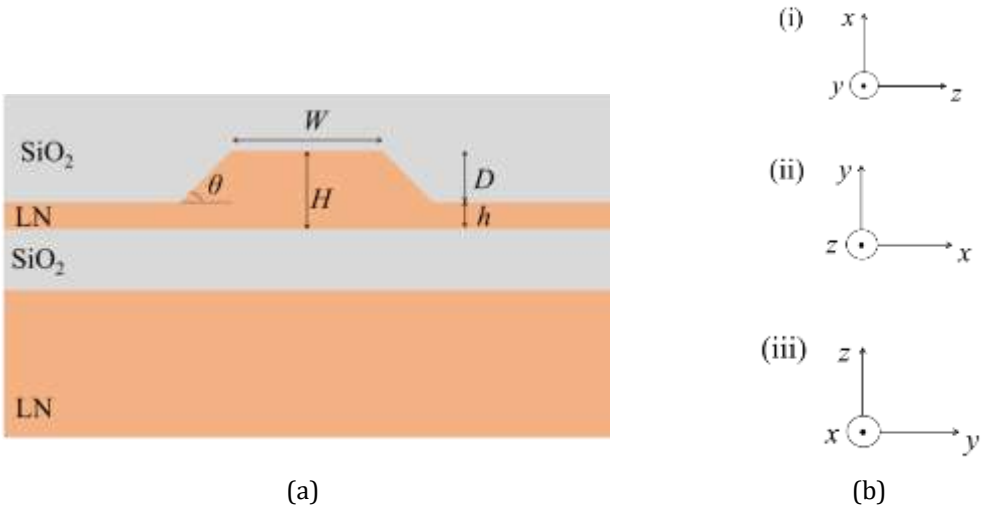

(a) (b)

Figure 2. (a) The cross section of the Lithium Niobate on insulator rib waveguide with θ = 75°. The principal dielectric axes orientation of the *x*-, *y*- and *z*-cut LN structure are represented in b(i)-(iii), respectively. In x-cut structure, the transverse field is confined in xz plane and propagates along the y direction. On the other hand, the transverse field is confined in *xy* (*yz*) plane with *z*(*x*) propagation direction in *y*-cut (*z*-cut) LN crystal structure.

$$n_{eff} = \frac{\beta_o}{\kappa_o} \tag{1}$$

3. RESULT AND DISCUSSION

3.1 Effective Refractive Indices

The initial investigation involved the modal phase matching as we set the pump and second harmonic wavelength at 1550 nm and 775 nm, respectively. From the result illustrated in Figure 3, the linear interaction between width of core, *w* and n_{eff} is found with $TE_{00,1550}$ reported the minimum value until its overlap with $TE_{20,775}$. As we set a wider value of w, the n_{eff} continuously increased and approaching the refractive indices of the core (n_{LN}), hence, increased the phase velocity of the mode. The modal phase matching condition is achieved as the n_{eff} of $TE_{00,1550}$ and $TE_{20,775}$ is set equal ($n_{eff,(TE00,1550)}$ - $n_{eff(TE20,775)}$). The similar finding is demonstrated over various crystal orientation with the *x*-cut reported the phase matching condition at narrower width of 0.53 μm followed with *z*-cut and *y*-cut, each at width of 0.6387 μm and 0.6493 μm. On top of that, we also observed the significant variation of n_{eff} over the crystal orientation with *z*- cut shows higher n_{eff} compared to others aided to stronger mode confinement. Hence, enhanced the conversion efficiency.

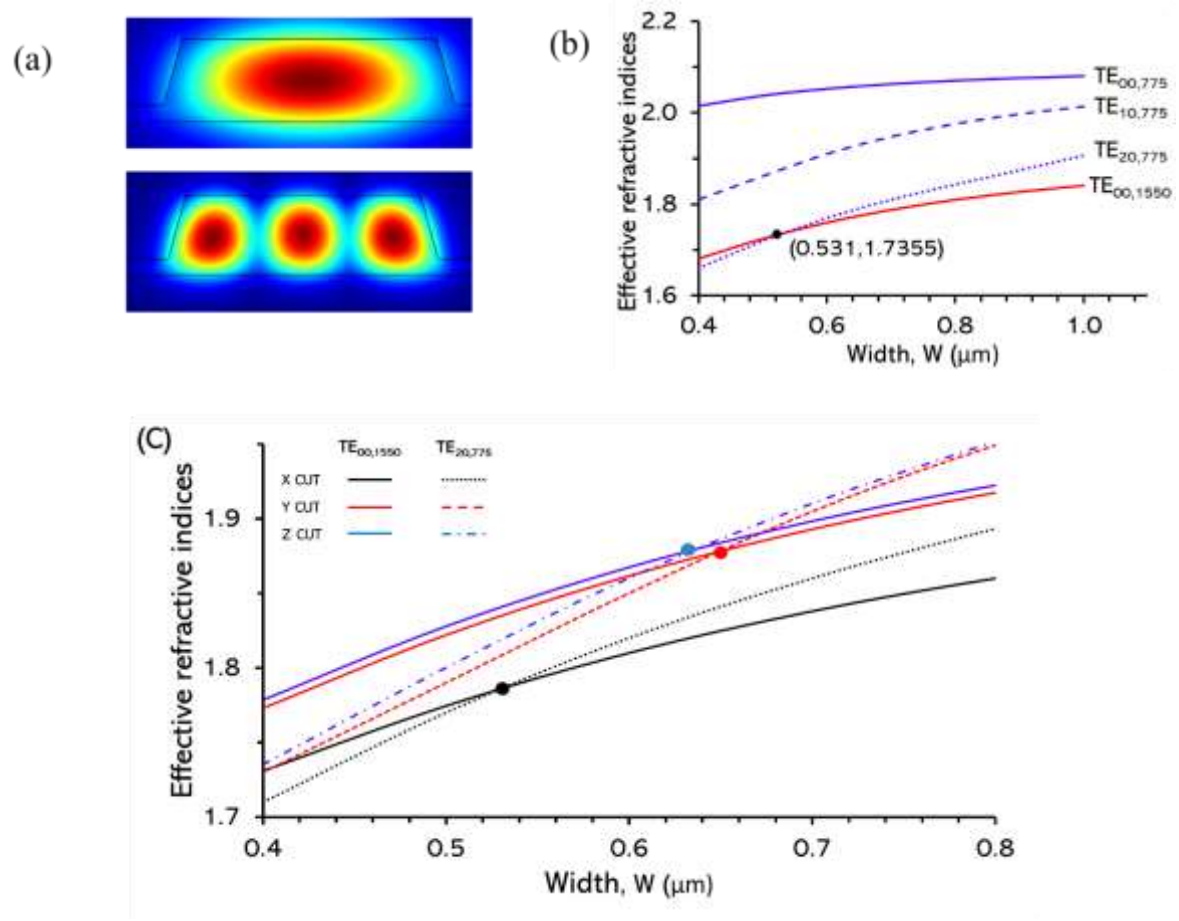

Figure 3. (a) Fundamental mode, TE_{00} and second order mode, TE_{20} profiles of the pump wavelength (1550 nm) and second harmonic wavelength (775 nm), respectively. The perfect phase matching condition achieved as the effective indices of TE_{00} overlapped with TE_{20} as depicted in (b). The effective indices overlapping between these modes on various crystal orientation are shown in (c) with the solid black, red and blue line indicate the fundamental mode indices of x-cut, y-cut and z-cut, respectively. Meanwhile, the dotted line represents the effective indices pattern of TE_{20}.

Additionally, the spatial mode profile is another important element that needs to take into consideration as it contributes to a significant enhancement of the optical waveguide efficiency. The spatial mode effective area, A_{eff} is calculated based on the following relation where $E_{1550,775}$ and χ^2 denotes the normalized field, over the *xz* transverse plane and second order waveguide region. As we switch from *x*-cut into the *y*-cut *(z*-cut), the partial differential is changed from *dxdz* into *dxdy* (*dydz*).

$$A_{eff} = \frac{\int_{-\infty}^{\infty} |E_{1550,775}|^2 dxdz}{\int_{\chi^2} |E_{1550,775}|^4 dxdz} \tag{2}$$

In Figure 4, the *x*-cut LNOI waveguide demonstrated a broader fundamental mode profile, $TE_{00,1550}$ compared to other followed with *z*-cut and *y*-cut structure. Due to the sharp refractive index contrast in vertical and horizontal direction, the symmetrical mode profile is found to be strongly confined at the center of the waveguide, contribute to the minimum frequency chirp which is beneficial for some optical application such as optical modulator. Eventually, broaden modal area reduced the spatial mode overlapping between $TE_{00,1550}$ and $TE_{20,775}$, hence diminished the coupling efficiency. Unlike $TE_{00,1550}$, $TE_{20,775}$ demonstrated lower electric field amplitude.

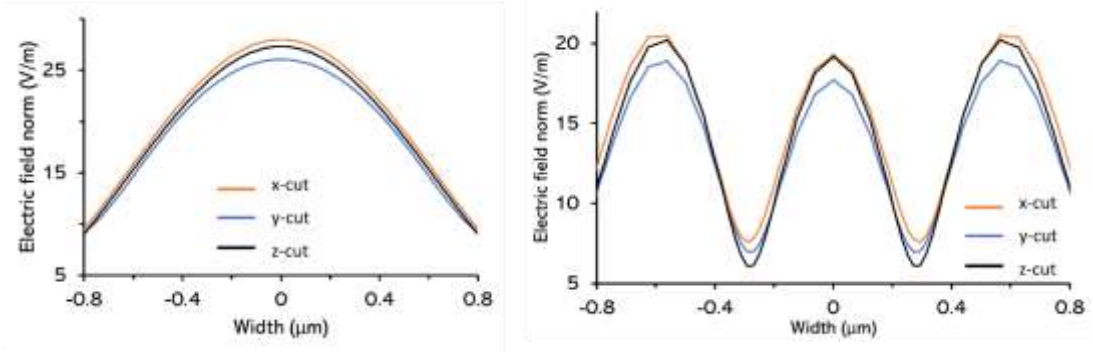

(a) (b)

Figure 4. (a) Fundamental mode, $TE_{00,1550}$ and (b) second order mode, $TE_{20,775}$ profiles at w = 1.5 μm. The x-cut, y-cut and z-cut crystal orientation represented by the orange, blue and black line, respectively.

3.2 Influence of Crystal Orientation Towards the Phase Matching Wavelength Tunability

The analysis is extended to observe the influence of crystal orientation over the phase matching wavelength tunability. We examine the spectral tuning curve dependence over width of core, w ranging from 400 to 900 nm, so that the phase matching condition is fulfilled within the desirable wavelength in telecommunication band. The relation between phase matching (PM) wavelength and width of core is presented in Figure 5. In general, the linear interaction between width and PM wavelength over different crystal orientation is reported with the wider width of core acquire a longer phase matching wavelength. In x-cut LNOI waveguide, the PM wavelength showed a slight increase within the telecom band ranging from 1390 to 1800 nm over the wider width of core. Interestingly, the z-cut structure offers broader wavelength tunability ranging from 1000 to 1800 nm. It is also noted that the significant wavelength increments with tuning slope of 2.06 is reported as w is set to be narrower than 0.75 μm. The strong interaction between ordinary mode, along y- axis and extraordinary mode, along z-axis facilitate the high polarization purity in z-cut LNOI waveguide, which later led to the significant PM wavelength tunability. This is in agreement with similar finding reported by other researchers (Luo, 2018) (Chen, 2020).

Unlike other crystal orientation, the phase matching condition of the y-cut LNOI waveguide is achieved at a maximum width of 0.65 μm within a narrower wavelength ranging from 1330 to 1550 nm. This could be attributed by the nonexistence of the polarization state interaction between the x- and y- axes which owned the ordinary mode, hence, act as isotropic material properties and possess lowest modulation efficiency. This condition can be improved by exploiting the x-axis to be the propagation axial; hence, the similar finding in z-cut is predicted to be demonstrated. Based on this result, it can be projected that the LNOI waveguide both in x- and z-crystal orientation suit for the fabrication of optical modulator which acquire broad wavelength tunability, with z-cut shows stronger modulation efficiency. This outcome is in agreement with the reported work for the fabrication of low loss ring resonator and optical modulator (Desiatov, 2019, Wu, 2018, Krasnokutska, 2019, Chen, 2021). Meanwhile, the acousto-optic based devices are reported to utilize the Y-cut LNOI structure which corresponds to our finding (Cai, 2019).

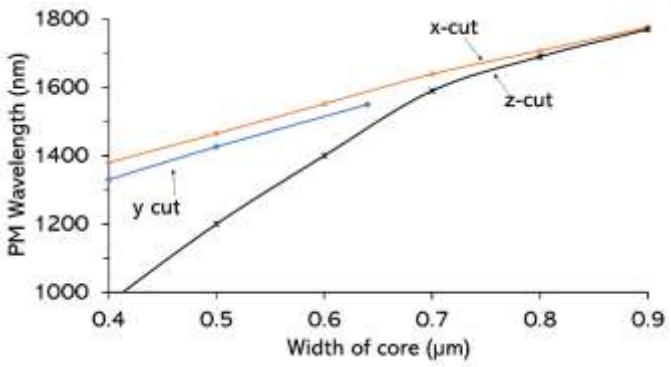

Figure 5. The influence of width of core towards the phase matching wavelength of the LNOI waveguide. The *x*-cut, *y*-cut and *z*-cut crystal orientation represented by the orange, blue and black line, respectively.

4. CONCLUSION

We have systematically demonstrated the phase matching condition on LNOI rib waveguide at FF and SH wavelength of 1550 nm and 775 nm to identify the relation of effective indices with the various crystal orientation. As we extend the analysis into a broader optical telecommunication region and by exploiting the strong interaction between two polarized modes ($TE_{00,1550}$ and $TE_{20,775}$), the broad PM wavelength tunability on *z*-cut and *x*-cut were reported. A slight variation in width of the waveguide contributes to significant wavelength shifting. Thus, a precise control during the fabrication is strongly require to achieve higher conversion efficiency. This numerical analysis able to provides a fundamental guideline to demonstrate the wavelength tunability of other nonlinear parametric process in LNOI waveguide structure such as difference frequency generation (DFG) and sum frequency generation (SFG) by employing the desire crystal orientation.

FUNDING

The research has been carried out under Long Term Research Grant Scheme project LRGS/1/2020/UM/01/5/2 provided by Ministry of Higher Education of Malaysia.

ACKNOWLEDGEMENTS

We thank Dr Karolina Slowik from Nicoulas Copernicus University in Torun and Assoc. Prof Dr Ahmad Rifqi for the theoretical advice and knowledge related to this project.

REFERENCES

[1] Wong, K.K. (Ed.). (2002). Properties of lithium niobate (No. 28). IET.
[2] Rao, A. and Fathpour, S. (2017). Compact lithium niobate electrooptic modulators. IEEE Journal of Selected Topics in Quantum Electronics, 24(4), 1-14.
[3] Qi, Y. and Li, Y. (2020). Integrated lithium niobate photonics. Nanophotonics, 9(6), 1287-1320.
[4] Pang, C., Li, R., Li, Z., Dong, N., Cheng, C., Nie, W., and Chen, F. (2018). Lithium Niobate Crystal with Embedded Au Nanoparticles: A New Saturable Absorber for Efficient Mode-Locking of Ultrafast Laser Pulses at 1 μm. Advanced Optical Materials, 6(16), 1800357.

[5] Alibart, O., D'Auria, V., De Micheli, M., Doutre, F., Kaiser, F., Labonté, L. and Tanzilli, S. (2016). Quantum photonics at telecom wavelengths based on lithium niobate waveguides. Journal of Optics, 18(10), 104001.

[6] Witmer, J.D., Valery, J.A., Arrangoiz-Arriola, P., Sarabalis, C. J., Hill, J. T. and Safavi-Naeini, A. H. (2017). High-Q photonic resonators and electro-optic coupling using silicon-on-lithium-niobate. Scientific reports, 7(1), 1-7.

[7] Mahmoud, M., Bottenfield, C., Cai, L., and Piazza, G. (2017, October). Fully integrated lithium niobate electro-optic modulator based on asymmetric Mach-Zehnder interferometer etched in LNOI platform. In 2017 IEEE Photonics Conference (IPC) (pp. 223-224). IEEE.

[8] Li, J., Yin, R., Ji, W., Huang, Q., Gong, Z., Lv, L., and Zhou, X. (2020). AWG optical filter with tunable central wavelength and bandwidth based on LNOI and electro-optic effect. Optics Communications, 454, 124445.

[9] Sun, D., Zhang, Y., Wang, D., Song, W., Liu, X., Pang, J., ... and Liu, H. (2020). Microstructure and domain engineering of lithium niobate crystal films for integrated photonic applications. Light: Science and Applications, 9(1), 1-18.

[10] Lacour, F., Courjal, N., Bernal, M.P., Sabac, A., Bainier, C., & Spajer, M. (2005). Nanostructuring lithium niobate substrates by focused ion beam milling. Optical materials, 27(8), 1421-1425.

[11] Levy, M., Osgood Jr, R.M., Liu, R., Cross, L.E., Cargill Iii, G.S., Kumar, A., & Bakhru, H. (1998). Fabrication of single-crystal lithium niobate films by crystal ion slicing. Applied Physics Letters, 73(16), 2293-2295.

[12] Saravi, S., Pertsch, T., & Setzpfandt, F. (2021). Lithium niobate on insulator: an emerging platform for integrated quantum photonics. Advanced Optical Materials, 9(22), 2100789.

[13] Xue, G.T., Niu, Y.F., Liu, X., Duan, J.C., Chen, W., Pan, Y., ... & Zhu, S. (2021). Ultrabright multiplexed energy-time-entangled photon generation from lithium niobate on insulator chip. Physical Review Applied, 15(6), 064059.

[14] Ye, X., Liu, S., Chen, Y., Zheng, Y., & Chen, X. (2020). Sum-frequency generation in lithium-niobate-on-insulator microdisk via modal phase matching. Optics Letters, 45(2), 523-526.

[15] Chen, J.Y., Sua, Y.M., Ma, Z.H., Tang, C., Li, Z., and Huang, Y.P. (2019). Efficient parametric frequency conversion in lithium niobate nanophotonic chips. OSA Continuum, 2(10), 2914-2924.

[16] Sanna, S. and Schmidt, W.G. (2010). Lithium niobate X-cut, Y-cut, and Z-cut surfaces from ab initio theory. Physical Review B, 81(21), 214116.

[17] Zelmon, D.E., Small, D.L., and Jundt, D. (1997). Infrared corrected Sellmeier coefficients for congruently grown lithium niobate and 5 mol.% magnesium oxide–doped lithium niobate. JOSA B, 14(12), 3319-3322.

[18] Luo, R., He, Y., Liang, H., Li, M., and Lin, Q. (2018). Highly tunable efficient second-harmonic generation in a lithium niobate nanophotonic waveguide. Optica, 5(8), 1006-1011.

[19] Chen, J.Y., Tang, C., Ma, Z.H., Li, Z., Sua, Y.M., and Huang, Y. P. (2020). Efficient and highly tunable second-harmonic generation in Z-cut periodically poled lithium niobate nanowaveguides. Optics Letters, 45(13), 3789-3792.

[20] Desiatov, B., Shams-Ansari, A., Zhang, M., Wang, C., & Lončar, M. (2019). Ultra-low-loss integrated visible photonics using thin-film lithium niobate. Optica, 6(3), 380-384.

[21] Wu, R., Wang, M., Xu, J., Qi, J., Chu, W., Fang, Z., ... & Cheng, Y. (2018). Long low-loss-litium niobate on insulator waveguides with sub-nanometer surface roughness. Nanomaterials, 8 (11), 910.

[22] Krasnokutska, I., Tambasco, J.L.J., & Peruzzo, A. (2019). Tunable large free spectral range microring resonators in lithium niobate on insulator. Scientific reports, 9(1), 1-7.

[23] Chen, G., Lin, H.L., Da Ng, J., & Danner, A.J. (2021). Integrated electro-optic modulator in z-cut lithium niobate thin film with vertical structure. IEEE Photonics Technology Letters, 33(23), 1285-1288.

[24] Cai, L., Mahmoud, A., & Piazza, G. (2019). Low-loss waveguides on Y-cut thin film lithium niobate: towards acousto-optic applications. Optics express, 27(7), 9794-9802.